



CHORUS

This is the accepted manuscript made available via CHORUS. The article has been published as:

Diffractive Imaging of C_{60} Structural Deformations Induced by Intense Femtosecond Midinfrared Laser Fields

Harald Fuest, Yu Hang Lai, Cosmin I. Blaga, Kazuma Suzuki, Junliang Xu, Philipp Rupp, Hui Li, Pawel Wnuk, Pierre Agostini, Kaoru Yamazaki, Manabu Kanno, Hirohiko Kono, Matthias F. Kling, and Louis F. DiMauro

Phys. Rev. Lett. **122**, 053002 — Published 6 February 2019

DOI: [10.1103/PhysRevLett.122.053002](https://doi.org/10.1103/PhysRevLett.122.053002)

Diffractive imaging of C₆₀ structural deformations induced by intense femtosecond mid-infrared laser fields

Harald Fuest,^{1,2} Yu Hang Lai,³ Cosmin I. Blaga,³ Kazuma Suzuki,⁴ Junliang Xu,³ Philipp Rupp,^{1,2} Hui Li,^{1,5,6} Pawel Wnuk,^{1,2,7} Pierre Agostini,³ Kaoru Yamazaki,⁸ Manabu Kanno,⁴ Hirohiko Kono,⁴ Matthias F. Kling,^{1,2,5} and Louis F. DiMauro³

¹*Physics Department, Ludwig-Maximilians-Universität Munich, D-85748 Garching, Germany*

²*Max Planck Institute of Quantum Optics, D-85748 Garching, Germany*

³*Department of Physics, The Ohio State University, Columbus, USA*

⁴*Department of Chemistry, Graduate School of Science, Tohoku University, Sendai 980-8578, Japan*

⁵*J.R. Macdonald Laboratory, Department of Physics,*

Kansas State University, Manhattan, Kansas 66506, USA

⁶*State Key Laboratory of Precision Spectroscopy, East China Normal University, Shanghai 200062, China*

⁷*Institute of Experimental Physics, Faculty of Physics, University of Warsaw, ul. Pasteura 5, 02-093 Warsaw, Poland*

⁸*Institute for Material Research, Tohoku University, 2-1-1 Katahira, Aoba-ku, Sendai 980-8577, Japan*

(Dated: November 16, 2018)

Theoretical studies indicated that C₆₀ exposed to linearly polarized intense infrared pulses undergoes periodic cage structural distortions with typical periods around 100 femtoseconds (1 fs = 10⁻¹⁵ s). Here, we use the laser-driven self-imaging electron diffraction technique, previously developed for atoms and small molecules, to measure laser-induced deformation of C₆₀ in an intense 3.6 μm laser field. A prolate molecular elongation along the laser polarization axis is determined to be (6.1 ± 1.4)% via both angular- and energy-resolved measurements of electrons that are released, driven back and diffracted from the molecule within the same laser field. The observed deformation is confirmed by density functional theory (DFT) simulations of nuclear dynamics on time-dependent adiabatic states and indicates a non-adiabatic excitation of the h_g(1) prolate-oblate mode. The results demonstrate the applicability of laser-driven electron diffraction methods for studying macromolecular structural dynamics in four dimensions with atomic time and spatial resolutions.

The 1985 discovery of C₆₀ by Kroto, Smalley and Curl [1] marked the beginning of fullerene research in nanoscience. This material class displays a remarkable structural variety of nanoscale-size shapes from simple spheres to tubules, onions, rods, ribbons etc., each possessing interesting, specific, and useful properties (see e.g. [2] and references therein). Since its discovery, the soccer ball shaped C₆₀ - the archetypical fullerene - remains the focus of most ongoing scientific studies aimed at unveiling its properties (see [3] for an in-depth review). The non-linear, nonresonant interaction of C₆₀ with strong femtosecond lasers has been the object of numerous investigations [4–13]. These studies revealed that at photon energies comparable with the separation between the first electronic excited state and the ground state (~1.6 eV [14]), an efficient transfer of laser energy into C₆₀'s internal degrees of freedom occurs via electronic and nuclear (vibrational) couplings. This extra energy is subsequently evaporated via C-C pair boil off, fragmenting the molecule over long time scales (from 0.5 ps up to μs). However, if the photon energy is not enough for single photon excitation, fragmentation is not observed even at high intensities (~10¹⁴ W/cm²) [15, 16]. In this regime, C₆₀ behaves like a macro-atom [10, 17], and many features are described well within the single active electron

picture without fragmentation. Nonetheless, fragmentation suppression does not imply a rigid cage. Indeed, theoretical models have shown that collective effects lead to periodic cage deformations along the laser polarization, with h_g(1) being the dominant active mode [18].

In this letter, we extend the laser-driven self-imaging electron diffraction techniques, previously developed for atoms [19–21] and small molecules [22–30] to directly image the elongation of C₆₀ induced by 80 TW/cm², 3.6 μm, 100 fs pulses. The observed deformation is confirmed by density functional theory (DFT) simulations of the nuclear dynamics on time-dependent adiabatic states. In contrast to the adiabatic electronic response to the applied field [15], the vibrational excitation is non-adiabatic (impulsive Raman), leading to a time delay of the structural response compared to the peak of the laser pulse profile. This result paves the way towards table-top, pump-probe real-time studies aimed at observing the complex dynamics of fullerenes and other macromolecular structures.

The goal of ultrafast molecular imaging is to visualize, interpret and ultimately control structural changes taking place during chemical reactions and biological processes. During the last two decades, various imaging approaches were developed to provide the required spatio-

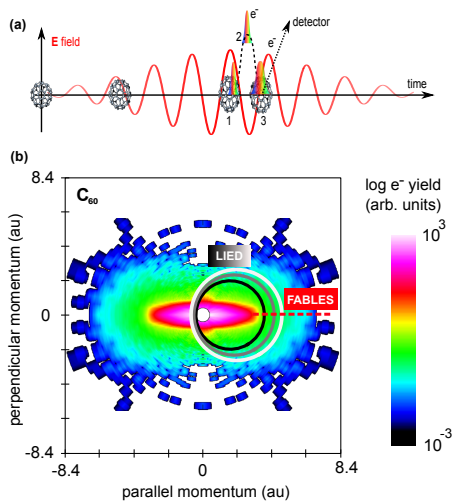


FIG. 1. The concept of ultrafast molecular imaging. (a) Illustration of the three-step LIED process and graphical illustration of C_{60} cage field-induced elongation during the pulse. (b) 2D photoelectron angular distribution data recorded for C_{60} irradiated with $3.6 \mu\text{m}$, 100 fs pulses at $80 \text{ TW}/\text{cm}^2$. The solid circles represent the integration area for LIED whereas the dashed line marks the area for FABLES (see text for details).

temporal resolutions, typically angstroms and femtoseconds, respectively (for a comprehensive review see [31] and references therein). Here, we employ laser-induced electron diffraction (LIED) [22, 24], a self-interrogating technique based on photoelectron recollision of electrons driven by strong laser fields. The method relies on a simple three step process [32, 33], illustrated in Fig. 1(a). In step (1), the laser launches the photoelectron into the continuum, ionizing the molecule. In step (2), the ejected photoelectron describes a field-driven quivering motion with the laser period. Finally, in step (3) the quivering photoelectron elastically recollides with its parent ion, encoding molecular structural information in the form of an elastic electron-ion differential cross section (DCS). LIED is therefore conceptually similar to the 80-year-old conventional gas-phase electron diffraction (CED) [34] technique but with the external electron beam replaced with the target’s own photoelectron. Once the DCS is extracted from the LIED experimental data, analysis and theoretical modeling for structural retrieval is performed using the tools employed in CED. The main advantage of LIED is its inherent temporal resolution. As the entire imaging process, from ionization to rescattering takes place during the pulse, the temporal resolution in LIED is shorter than the femtosecond pulse itself. In fact, in select cases LIED provides resolutions as short as a single laser cycle. In [25], a sub-cycle, 5 fs temporal resolution was achieved even though mid-infrared laser pulses with durations in the 50-60 fs range (FWHM) at various

wavelengths were used. On the other hand, the spatial resolution, both in LIED as in CED is determined by the momentum transfer of the scattering electron and previous studies have shown that for LIED 100 eV electron energies suffice to produce the resolutions necessary for molecular dynamics studies [24].

A single 100 fs midinfrared pulse is sufficient to both distort and image the distortion of C_{60} molecules while providing an effective 40-50 fs temporal resolution. Two key ingredients make this possible. On one hand, photoionization with midinfrared pulses is a high order non-linear process that is effective only near the peak of the laser pulse (see Supplement Material and the included references [18, 35–42]). Therefore, the cage “sees” a returning photoelectron only during 3-4 laser cycles at the peak of the pulse envelope when the imaging photoelectron is ionized efficiently. On the other hand, the excitation of the 125 fs $h_g(1)$ mode is a two photon impulsive Raman process, effective during most of the laser pulse [18]. Thus, the imaging experiment reported here happens during the first half of the 100 fs laser pulse: first, during ramp up the undistorted cage is two-photon impulsively Raman excited with increasing efficiency followed by LIED imaging at the peak of the pulse (within 3-4 laser cycles). Although excitation continues during ramp down, strong field ionization is inefficient and even if present, it only produces low energy electrons that do not contribute to the extracted DCS. We also point out that the 100 fs midinfrared pulse has sufficient bandwidth to allow efficient impulsive Raman excitation of the $h_g(1)$, 125 fs period dominant mode and that adjusting pulse durations or intensities could provide an effective way to measure cage distortions at various degrees of excitation.

Based on the three-step model, two techniques were introduced to obtain structural information. In the first method, called angle-swept LIED, accurate elastic electron-ion DCS were extracted from 2D photoelectron angular distributions [19]. This method employs an identical structural retrieval procedure as in conventional electron diffraction (CED), where an electron beam produced by an external gun is used [34]. The second method, dubbed fixed-angle broadband laser-driven electron scattering (FABLES) [26] does not have a direct CED analogue. Instead, it is similar to white light interferometry as it takes advantage of the broadband nature of the rescattered electron wavepacket, requiring only detection of the photoelectron spectrum emitted along the laser polarization (backscattering geometry). The structural information is retrieved via rectification using a simple 1D-Fourier transformation of the energy-dependent DCS. For both methods, an independent atom model (IAM) is adopted, a theoretical tool based on the approximation that for collision energies approaching 100 eV and above, the DCS is given by a coherent summation of independent atomic scattering waves. The DCS extraction procedure from experimental 2D angular distributions as

well as IAM data modeling are detailed in previous work [24–26]. Here, C_{60} imaging is realized independently via both LIED and FABLES methods. To obtain electron recollision energies with suitable resolving power while keeping the laser intensity below the saturation intensity of C_{60} (80 TW/cm² [15]), mid-infrared driving lasers operating at wavelengths around 3 μ m are ideal. Below this limit, the resolving power is insufficient, whereas longer wavelengths lead to significantly lower scattering cross sections due to higher electron energies and increased transverse wave packet spread [35]. Conceptually, the experiment is depicted in Fig. 1. To image the predicted cage deformation induced by the laser pulse as illustrated in Fig. 1(a), the 2D photoelectron angular distribution was measured (Fig. 1(b)). For both LIED and FABLES, only electrons detected with energies in excess of 100 eV are counted. Therefore, if thermionic emission is present, its low-energy contribution peaked at 0 eV and extending up to 20 eV [43] has no effect on the imaging methods employed here. We find that the structural information embedded in the 2D photoelectron distribution is that of the elongated cage and it can be retrieved via LIED or FABLES (in the form of photoelectron yields along the circles and the dashed line indicated in Fig. 1(b), respectively).

The laser system is detailed in the SI. Briefly, mid-infrared fields are generated by an optical parametric amplifier delivering 100 fs, up to 150 μ J, 2.9–4.2 μ m tunable linearly polarized pulses at 1 kHz repetition rate. The C_{60} target was sublimated from a high-temperature (≤ 650 °C) oven into an ultra-high vacuum chamber (10^{-8} torr). The photoelectron spectra were recorded in a time-of-flight spectrometer operated in a field-free electron detection mode with an angular acceptance of $\sim 2.1^\circ$. Operated in ion detection mode, the spectrometer collected the mass spectrum of C_{60} to confirm the lack of fragmentation (cf. Figure S1 of the SI).

From the 2D angular distribution (see SI for details), DCS for electron scattering energies of 70, 80 and 90 eV were extracted by integrating the measured yield within 3.5, 5 and 6.5% around the mean value, respectively. Rescattering energies below 70 eV were discarded since IAM is not expected to produce reliable quantitative results, whereas above 100 eV the detected yield was too low, limiting the signal-to-noise ratio. For each extracted DCS, large sets of IAM calculations for a wide range of cage deformations were benchmarked against experimental measurements (cf. Fig. 2). This procedure is based on assessing the angular positions of the DCS diffraction minima and maxima of the experiment (upper panel Fig. 2) to the corresponding theoretical values calculated for a wide range of cage elongations, shown in the lower panel of Fig. 2. The best match for each extremum is indicated by a circle placed on the corresponding curve. This analysis yields four elongation values for the four identified extrema: 6%, 5%, 4% and 7%, from the highest

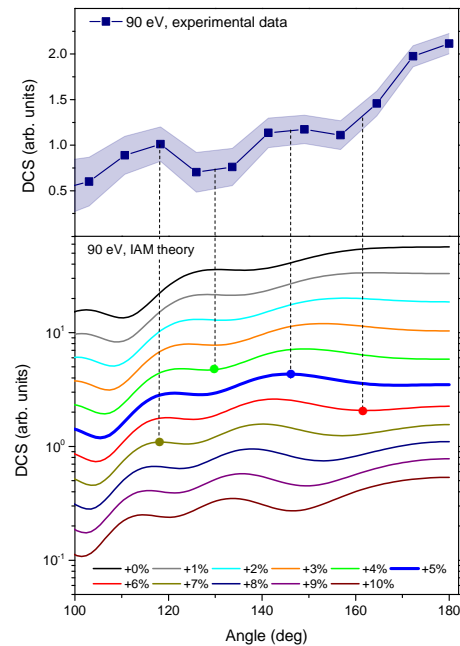


FIG. 2. Comparison of elastic DCS from experimental LIED data (upper panel) versus IAM calculation (lower panel) at 90 eV. Each line in the lower panel corresponds to a cage elongated along the laser polarization by the value indicated in the legend with respect to the field-free, spherical cage. The minima and maxima indicated in the figure are diffraction extremes, whose angular positions are determined by the size of the cage. The four circles indicate the elongations that best match the corresponding experimental values. From the highest angle to the lowest angle extrema, the elongations are 6%, 5%, 4% and 7%.

to the lowest angle, respectively. The identical procedure for 80 and 70 eV DCS yield two additional elongations for each DCS: (2%, 2%) and (5%, 4%), respectively. Therefore, we infer from our LIED analysis that at the peak of the laser field the C_{60} cage has a prolate shape with an elongation estimated to be $(4.2 \pm 1.9)\%$ or $+(30 \pm 13)$ pm for an unperturbed cage diameter of 7 Å. The FABLES data, obtained in back-scattering geometry, provides a more direct estimation of the field-induced elongation. We used kinetic energies up to 800 eV to retrieve the experimental molecular contrast factor, the scattering interference term in CED [34], shown as solid blue line in Fig. 3. The best fit is realized for an elongation of $(8 \pm 2)\%$. Both LIED and FABLES data sets indicate a prolate C_{60} geometry under the influence of the laser field with a combined averaged elongation of $(6.1 \pm 1.4)\%$ or (43 ± 10) pm. Unlike previous FABLES data analysis [26], a different error analysis is used here. Since the result depends on the entire photoelectron spectrum, the influence of a single TDC-bin is weighted by the counts accumulated in it. Following this procedure, the bins at high energies are contributing less to the retrieval. In comparison to the standard analysis this procedure led

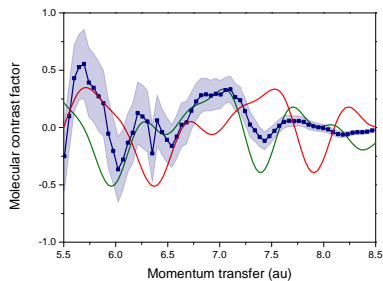


FIG. 3. Results for FABLES. Experimental data extracted from the photoelectron spectrum along the laser polarization (FABLES) are shown as blue symbols with associated statistical errors (shaded area). The unperturbed cage theoretical prediction is shown in red, whereas the best theoretical fit with the cage elongation as fit parameter is shown in green ($8\pm 2\%$).

to similar results for C_{60} , but with improved robustness to statistical noise. We point out that inferring this result relies on IAM’s accuracy to reproduce the DCS of C_{60} . In [25], in the case of N_2 , the 100 eV DCS produced a ~ 5 pm error, a result that was possible because for this small molecule IAM was accurately optimized and benchmarked against conventional DCS data. Here, no conventional DCS data exists for electrons scattering at large angles at the energies employed. Therefore, the IAM calculations shown in Fig. 2 are likely less accurate due to the increase in the number of neighbors for an atom (59 for C_{60} vs. 1 for N_2). Future CED experimental measurements and theoretical advances for DCS modeling could improve the precision reported here.

Theoretical support for the measurements reported here is provided at the standard B3LYP/6-31G(d) level DFT and at the self-consistent charge density-functional based tight-binding (SCC-DFTB) semi-empirical molecular orbital theory [41, 44] combined with the standard mio-1-1 CC parameter set [44] (for details see SI). At a peak intensity of 80 TW/cm^2 for $3.6 \mu\text{m}$, 60 fs (FWHM) pulses, both theoretical methods show a prolate-oblate molecular oscillation with a 125 fs period, as seen in Fig. 4(a). The oscillation is determined by the dominant mode, the five-fold degenerate prolate-oblate $h_g(1)$ mode of neutral C_{60} , $T_{h_g(1)}=125$ fs. The oscillatory amplitude reaches 1.7% during the pulse (DFT result). Significant damping of the oscillation is not observed even up to 15 ps. The temporal profile of the elongation indicates a non-adiabatic response to the pulse envelope, with a maximum emerging ~ 20 fs after the peak of the laser pulse. In the experiment, the ionization and therefore the imaging “snapshot” via rescattering reach a maximum around the peak of the laser pulse. Consequently, LIED and FABLES view the C_{60} molecule near its maximum elongation in prolate geometry. As the 120 fs prolate-oblate oscillatory motion is an intrinsic molecular property, imag-

ing the cage elongation while scanning the duration of the laser pulse would allow measuring the damping factors and in turn uncover the complex intramodal coupling, where the energy initially stored primarily in the $h_g(1)$ mode leaks into other modes. Theoretical support toward this goal is shown in Fig. 4b, where the maximum elongation is plotted as a function of charge state, wavelength, and pulse duration. The magnitude of deformation is nearly identical for 3.1 and $3.6 \mu\text{m}$ and it shows only a weak dependence on the molecular charge state. This is unsurprising, as the driving wavelengths are non-resonant and the removal of a small number i of electrons does not appreciably alter the internuclear forces determined by the remaining $(240-i)$ valence electrons. However, the maximum elongation changes appreciably with the pulse duration, decreasing over 20% as the pulse doubles in length from its peak value at ~ 70 fs towards 150 fs (the Raman excitation becomes less efficient as the pulse bandwidth is reduced). Finally, we note that although experiment and theory conclusively observed the elongation of the cage, the agreement is not quantitatively perfect, likely caused by DCS modeling via IAM as described above. DCS modeling with more realistic assumptions such as the Schwinger multichannel method which includes interference effects due to Bragg-type electron diffraction on the C_{60} cage [45] could improve the agreement between experiment and theory.

In conclusion, we have extended laser-driven ultrafast molecular imaging from atoms and small molecules to C_{60} , visualizing its structural deformation induced by an intense mid-infrared laser field on femtosecond time scales. Numerical DFT and DFTB simulations indicate that the deformation originates from non-adiabatic excitation of the $h_g(1)$ prolate-oblate mode. Our results pave the way towards recording macromolecular structures and dynamics with atomic time and spatial resolutions in a pump-probe table-top setup as obtained for acetylene [30].

We acknowledge fruitful discussions with Lew Cocke, Chii-Dong Lin, Itzik Ben-Itzhak, Kiyoshi Ueda, and Jens Biegert. The experimental work was conducted at OSU, and supported by the U.S. Department of Energy, Office of Science, Basic Energy Sciences, under Award #DE-GF02-04ER15614. The JRML personnel was supported by the same agency under Award #DE-FG02-86ER13491. H.F., P.R., H.L, and M.F.K. are grateful for support by the German Research Foundation (DFG) via the cluster of excellence Munich Centre for Advanced Photonics and by the European Union (EU) via the European Research Council (ERC) grant ATTOCO. H.K. acknowledges support by JSPS KAKENHI Grant Number JP16H04091. C.I.B. acknowledges supported by the Air Force Office of Scientific Research under MURI, Award No. FA9550-16-1-0013. K. Y. is grateful for the financial supports from Building of Consortia for the Development of Human Resources in Science and Technology, MEXT.

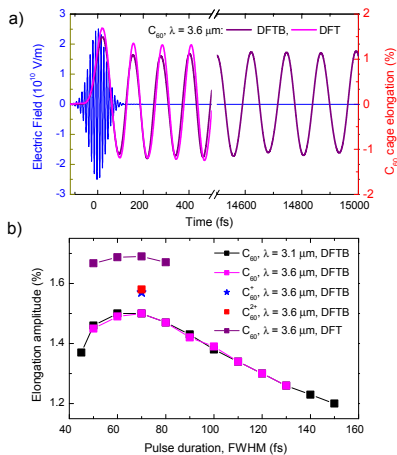


FIG. 4. Density-functional theory results. a) Temporal profile of the elongation $[d(t)/d_{eq}]-1$ (DFT- magenta, DFTB - purple) of neutral C_{60} in a mid-infrared Gaussian pulse (blue line) at peak intensity $I_0=80$ TW/cm², 60 fs duration, and 3.6 μm wavelength. Here, $d(t)$ is the length of C_{60} along the polarization direction of the applied field and d_{eq} is its equilibrium value. b) Elongation as a function of charge species, wavelength, and pulse duration. Simulations to obtain the values of field-induced distortion are carried out by using the time-dependent adiabatic state approach [18] combined with the SCC-DFTB method (mio-1-1 parameter set). The time step Δt was chosen to be 0.1 fs. Black squares show values at $\lambda=3.1$ μm for neutral C_{60} and magenta squares at $\lambda=3.6$ μm . The blue star symbol indicates the value for C_{60}^+ and the red square symbol indicates the value for C_{60}^{2+} . The value for $\lambda=3.6$ μm is also evaluated by B3LYP/6-31G(d) of DFT, indicated by the purple square symbol.

IAM modeling was performed with CPU time awarded by the Ohio Supercomputer Center (Project No. PAS0207).

[1] H. W. Kroto, J. R. Heath, S. C. O'Brien, R. F. Curl, and R. E. Smalley, *Nature* **318**, 162 (1985).
 [2] K. D. Sattler, *Handbook of nanophysics: Clusters and fullerenes*. (CRC Press, Boca Raton, 2015).
 [3] F. Lépine, *J. Phys. B* **48**, 122002 (2015).
 [4] M. Tchapyguine, K. Hoffmann, O. Dühr, H. Hohmann, G. Korn, H. Rottke, M. Wittmann, I. V. Hertel, and E. E. B. Campbell, *J. Chem. Phys.* **112**, 2781 (2000).
 [5] E. E. B. Campbell, K. Hoffmann, H. Rottke, and I. V. Hertel, *J. Chem. Phys.* **114**, 1716 (2001).
 [6] I. V. Hertel, T. Laarmann, and C. P. Schultz, *Adv. At. Mol. Opt. Phys.* **50**, 219 (2005).
 [7] I. Shchatsinin, T. Laarmann, N. Zhavoronkov, C. P. Schulz, and I. V. Hertel, *J. Chem. Phys.* **129**, 204308 (2008).
 [8] I. V. Hertel, I. Shchatsinin, T. Laarmann, N. Zhavoronkov, H. H. Ritzke, and C. P. Schulz, *Phys. Rev. Lett.* **102**, 023003 (2009).

[9] R. A. Ganeev, L. B. E. Bom, J. Abdul-Hadi, M. C. H. Wong, J. P. Brichta, V. R. Bhardwaj, and T. Ozaki, *Phys. Rev. Lett.* **102**, 013903 (2009).
 [10] Y. Huismans, E. Cormier, C. Cauchy, P. A. Hervieux, G. Gademann, A. Gijsbertsen, O. Ghafur, P. Johnson, P. Logman, T. Barillot, C. Bordas, F. Lépine, and M. J. J. Vrakking, *Phys. Rev. A* **88**, 013201 (2013).
 [11] R. A. Ganeev, C. Hutchison, T. Witting, F. Frank, S. Weber, W. A. Okell, E. Fiordilino, D. Cricchio, F. Persico, A. Zair, J. W. G. Tisch, and J. P. Marangos, *J. Opt. Soc. Am. B* **30**, 7 (2013).
 [12] H. Li, B. Mignolet, G. Wachter, S. Skruszewicz, S. Zherebtsov, F. Süßmann, A. Kessel, S. A. Trushin, N. G. Kling, M. Kübel, B. Ahn, D. Kim, I. Ben-Itzhak, C. L. Cocke, T. Fennel, J. Tiggesbäumker, K.-H. Meiwes-Broer, C. Lemell, J. Burgdörfer, R. D. Levine, F. Remacle, and M. F. Kling, *Phys. Rev. Lett.* **114**, 123004 (2015).
 [13] H. Li, B. Mignolet, Z. Wang, K. J. Betsch, K. D. Carnes, I. Ben-Itzhak, C. L. Cocke, F. Remacle, and M. F. Kling, *J. Phys. Chem. Lett.* **7**, 4677 (2016).
 [14] A. Sassara, G. Zerza, and M. Chergui, *Chem. Phys. Lett.* **261**, 213 (1996).
 [15] V. R. Bhardwaj, P. B. Corkum, and D. M. Rayner, *Phys. Rev. Lett.* **91**, 203004 (2003).
 [16] V. R. Bhardwaj, P. B. Corkum, and D. M. Rayner, *Phys. Rev. Lett.* **93**, 043001 (2004).
 [17] M. Ruggenthaler, S. V. Popruzhenko, and D. Bauer, *Phys. Rev. A* **78**, 033413 (2008).
 [18] K. Nakai, H. Kono, Y. Sato, N. Niitsu, R. Sahnoun, M. Tanaka, and Y. Fujimura, *Chem. Phys.* **338**, 127 (2007).
 [19] M. Okunishi, T. Morishita, G. Prümper, K. Shimada, C. D. Lin, S. Watanabe, and K. Ueda, *Phys. Rev. Lett.* **100**, 143001 (2008).
 [20] D. Ray, B. Ulrich, I. Bocharova, C. Maharjan, P. Ranitovic, B. Gramkow, M. Magrakvelidze, S. De, I. V. Litvinyuk, A. T. Le, T. Morishita, C. D. Lin, G. G. Paulus, and C. L. Cocke, *Phys. Rev. Lett.* **100**, 143002 (2008).
 [21] J. Xu, C. I. Blaga, A. D. DiChiara, E. Sistrunk, K. Zhang, Z. Chen, A.-T. Le, T. Morishita, C. D. Lin, P. Agostini, and L. F. DiMauro, *Phys. Rev. Lett.* **109**, 233002 (2012).
 [22] T. Zuo, A. D. Bandrauk, and P. B. Corkum, *Chem. Phys. Lett.* **259**, 313 (1996).
 [23] M. Meckel, D. Comtois, D. Zeidler, A. Staudte, D. Pavičić, H. C. Bandulet, H. Pépin, J. C. Kieffer, R. Dörner, D. M. Villeneuve, and P. B. Corkum, *Science* **320**, 1478 (2008).
 [24] J. Xu, Z. Chen, A.-T. Le, and C. D. Lin, *Phys. Rev. A* **82**, 033403 (2010).
 [25] C. I. Blaga, J. Xu, A. D. DiChiara, E. Sistrunk, K. Zhang, P. Agostini, T. A. Miller, L. F. DiMauro, and C. D. Lin, *Nature* **483**, 194 (2012).
 [26] J. Xu, C. I. Blaga, K. Zhang, Y. H. Lai, C. D. Lin, T. A. Miller, P. Agostini, and L. F. DiMauro, *Nat. Commun.* **5**, 4635 (2014).
 [27] M. G. Pullen, B. Wolter, A.-T. Le, M. Baudisch, M. Hemmer, A. Senftleben, C. D. Schröter, J. Ullrich, R. Moshhammer, C. D. Lin, and J. Biegert, *Nat. Commun.* **6**, 7262 (2015).
 [28] Y. Ito, C. Wang, A. Le, M. Okunishi, D. Ding, C. D. Lin, and K. Ueda, *Struct. Dyn.* **3**, 034303 (2016).
 [29] M. G. Pullen, B. Wolter, A.-T. Le, M. Baudisch,

- M. Sclafani, H. Pires, C. D. Schröter, J. Ullrich, Moshhammer, T. Pfeifer, C. D. Lin, and J. Biegert, *Nat. Commun.* **7**, 11922 (2016).
- [30] B. Wolter, M. G. Pullen, A.-T. Le, M. Baudisch, K. Doblhoff-Dier, A. Senftleben, M. Hemmer, C. D. Schröter, J. Ullrich, T. Pfeifer, R. Moshhammer, S. Gräfe, O. Vendrell, C. D. Lin, and J. Biegert, *Science* **354**, 308 (2016).
- [31] J. Xu, C. I. Blaga, P. Agostini, and L. F. DiMauro, *J. Phys. B* **49**, 112001 (2016).
- [32] K. J. Schafer, B. Yang, L. F. DiMauro, and K. C. Kulander, *Phys. Rev. Lett.* **70**, 1599 (1993).
- [33] P. B. Corkum, *Phys. Rev. Lett.* **71**, 1994 (1993).
- [34] I. Hargittai and M. Hargittai, *Stereochemical Applications of Gas-Phase Electron Diffraction, Part A*. (John Wiley & Sons, Hoboken, 1988).
- [35] P. Colosimo, G. Doumy, C. I. Blaga, J. Wheeler, C. Hauri, F. Catoire, J. Tate, R. Chirila, A. M. March, G. G. Paulus, H. G. Muller, and P. A. . L. F. DiMauro, *Nat. Phys.* **4**, 386 (2008).
- [36] M. V. Ammosov, N. B. Delone, and V. P. Krainov, *Sov. Phys. JETP* **64**, 1191 (1986).
- [37] G. K. Paramonov, O. Kühn, and A. D. Bandrauk, *Phys. Chem. A* **120**, 3175 (2016).
- [38] C. I. Blaga, F. Catoire, P. Colosimo, G. G. Paulus, H. G. Muller, P. Agostini, and L. F. DiMauro, *Nature Physics* **5**, 335 (2009).
- [39] N. Niitsu, M. Kikuchi, H. Ikeda, K. Yamazaki, M. Kanno, H. Kono, K. Mitsuke, M. Toda, and K. Nakai, *J. Chem. Phys.* **136**, 164304 (2012).
- [40] M. J. Frisch and et.al., Gaussian 09, Gaussian, Inc. Wallingford, CT (2009).
- [41] B. Aradi, B. Hourahine, and T. Frauenheim, *J. Phys. Chem. A* **111**, 5678 (2007).
- [42] X. Zhou, Z. Lin, C. Jiang, M. Gao, and R. E. Allen, *Phys. Rev. B* **82**, 075433 (2010).
- [43] E. E. Campbell, K. Hansen, K. Hoffmann, G. Korn, M. Tchapyguine, M. Wittmann, and I. V. Hertel, *Phys. Rev. Lett.* **84**, 2128 (2000).
- [44] M. Elstner, D. Porezag, G. Jungnickel, J. Elsner, M. Haugk, T. Frauenheim, S. Suhai, and G. Seifert, *Phys. Rev. B* **58**, 7260 (1998).
- [45] L. R. Hargreaves, B. Lohmann, C. Winstead, and V. McKoy, *Phys. Rev. A* **82**, 062716 (2010).